Biophysical Journal
Article

Biophysical Society

Interference between Triplex and Protein Binding to Distal Sites on Supercoiled DNA

Agnes Noy,[1] Anthony Maxwell,[2] and Sarah A. Harris[3,4,*]
[1]Department of Physics, Biological Physical Sciences Institute, University of York, York, United Kingdom; [2]Department of Biological Chemistry, John Innes Centre Norwich Research Park, Norwich, United Kingdom; [3]School of Physics and Astronomy and [4]Astbury Centre for Structural and Molecular Biology, University of Leeds, Leeds, United Kingdom

ABSTRACT We have explored the interdependence of the binding of a DNA triplex and a repressor protein to distal recognition sites on supercoiled DNA minicircles using MD simulations. We observe that the interaction between the two ligands through their influence on their DNA template is determined by a subtle interplay of DNA mechanics and electrostatics, that the changes in flexibility induced by ligand binding play an important role and that supercoiling can instigate additional ligand-DNA contacts that would not be possible in simple linear DNA sequences.

INTRODUCTION

While the structural information available for protein-DNA interactions at the atomistic level has mostly been obtained for linear short DNA fragments, in vivo protein-DNA interactions occur in a variety of complex structural topologies like DNA loops or hierarchical chromatin. One of the most ancient and elemental cellular strategies to organize genomes structurally is DNA supercoiling (1). The over- or underwinding of DNA emerges from several cellular processes that induce torsional stress either by sequentially separating the two strands (transcription and replication) (2) or by wrapping DNA around proteins (such as in the nucleosome (3) and by interaction with DNA gyrase (4,5)). The latter, together with the use of ATP, usually serve to maintain an homeostatically underwound state in eukaryotes (6) and prokaryotes (7), respectively. Recently, it has been shown that, in eukaryotes, different levels of superhelical stress can be restrained on chromatin fibers depending upon the precise organization of the nucleosome units (6,8).

The relaxed twist of an unconstrained double-stranded DNA helix is characterized by its default linking number (Lk_0), which is the number of times one strand of the double helix is wrapped around the other. This is equivalent to the helical twist (Tw), or to the number of basepairs divided by the helical repeat. However, when DNA is over- or underwound and topologically constrained, the resultant torsional stress is relieved either by 1) the introduction of writhe (Wr), which is the coiling of the DNA helix around itself, or 2) by changes in the molecular helical twist (Tw). In this case, the total Lk of the fragment, which has been shifted away from Lk_0 ($\Delta Lk = Lk - Lk_0$), is distributed between Tw and Wr according to the topological condition that $Lk = Tw + Wr$. The superhelical density (σ), which is the normalization of ΔLk ($\sigma = \Delta Lk/Lk_0$), is the parameter used to quantify the degree of supercoiling within the DNA (9). In prokaryotes, levels of supercoiling are $\sim\sigma = -0.06$ to $\sigma = -0.075$ (7) and, in eukaryotes, supercoiling levels between $\sigma = -0.09$ and -0.06 have been detected, depending on the specific organization of chromatin fibers (8).

DNA supercoiling influences gene regulation by altering both the global and the local structure of the helix. DNA undertwisting caused by negative supercoiling can promote the melting of the double helix (10) by weakening base stacking (11) and, thus, facilitates the formation of the open complex during transcription. Moreover, supercoiling also affects DNA recognition by proteins through changes in its fine structure that perturb unspecific contacts within the so-called indirect-readout mechanism of binding (12). The bacteriophage 434 repressor is an example of this because its binding to DNA causes local overtwisting within the central basepairs (bp) of the operator, which are not contacted by the protein (13). The interaction with other molecules such as drugs or different types of nucleic acids can also be influenced by levels of supercoiling. For example, the formation of triplex DNA has been demonstrated to be more efficient for negatively supercoiled DNA, and this property has been subsequently successfully exploited to develop an assay for reporting topoisomerase activity (14).

Submitted July 28, 2016, and accepted for publication December 16, 2016.
*Correspondence: s.a.harris@leeds.ac.uk
Editor: Tamar Schlick.
http://dx.doi.org/10.1016/j.bpj.2016.12.034

In closed DNA loops, changes in superhelical stress have been seen to alter the physical properties of distal sites on DNA, such as in the human MYC proto-oncogen (15) and in the leu-ABCD-leuO-ilv1H region of *Salmonella* (16), where supercoiling signal is transmitted along a series of far regulatory elements or genes, creating a mechanism to transfer biological information for modulating gene expression beyond transcription-factor recognition (17). Recently, multiscale simulations on DNA minicircles containing ~100 bp have revealed a physical coupling across the whole circle achieved by the transmission of mechanical stress through the molecule of DNA itself (10). Allostery on unconstrained DNA has also been proved in that the binding of a protein can be influenced by another protein bound nearby within a length of 20 bp (18).

Under physiological conditions, torsionally stressed DNA is packed into plectonemes (or interwound superhelices). These structures have the property to bring widely distant sites (up to kilo-basepairs) into close proximity, playing a crucial role in gene regulation by promoting enhancer-promoter communication (19). Single molecule experiments have shown that DNA loops bridged by proteins such as the lac (20) or the phage lambda (21) repressors are facilitated by supercoiling and that the transition between close and open states is sharper in plectonemes compared to non-supercoiled loops, creating an all-or-nothing response because of small changes of protein concentration (21,22). The formation of closed DNA loops through DNA-protein-DNA bridges by lac, gal, or phage lambda repressors has also been seen sufficient for dividing a DNA fragment into different topological domains (23). Finally, molecular dynamics (MD) simulations of DNA minicircles bound to the human topoisomerase IB also observed the formation of a DNA-protein bridge, due to interactions between positively charged lysine residues far from the canonical DNA binding domain and a DNA site across the minicircle (24). We have further discussed the importance of protein-DNA interactions in supercoiled topoisomers in a recent review (25).

Here, we explore the interdependence of the binding of two ligands (a DNA triplex and the bacteriophage 434 repressor) to separated (one helical-turn apart) recognition sites on supercoiled DNA minicircles, and make a series of predictions testable in the laboratory. We investigate action-at-a-distance between both sites considering one-dimensional (1D) communication, which is through the DNA fiber itself and three-dimensional (3D) communication, which is across supercoiled DNA loops. We have used MD simulations to observe the structural and dynamic changes on binding subsequent ligands to a 260 bp minicircle constrained at four different levels of supercoiling through the formation of four topoisomers: $\Delta Lk = -2$ with $\sigma = -0.069$, $\Delta Lk = -1$ with $\sigma = -0.027$, $\Delta Lk \approx 0$ (relaxed), and $\Delta Lk = +1$ with $\sigma = 0.058$ (for more details about σ-calculation, see Sutthibutpong et al. (26)), using both implicitly and explicitly solvated MD simulations. Minicircles of this size are sufficiently small to be accessible to atomistic MD simulations (27), but can also be synthesized enzymatically (28). Moreover, because both triplex and 434-repressor binding have been previously demonstrated to be sensitive to supercoiling (13,14), this provides a particularly tractable system for comparing theoretical predictions with future experimental results.

MATERIALS AND METHODS

Construction of DNA minicircles

Linear 260 bp DNA sequences were built using the NAB module implemented in AmberTools12 (29). The DNA sequence was designed using the minicircles synthesized by Fogg et al. (28). However, the original 251 bp sequence was modified to contain a 16 bp triplex binding site (TCTCTCTCTCTCTCTC), which forms T.AT and C+.GC triplets with eight additional negative charges, and a 14 bp, 434-phage repressor binding site (30) separated by approximately one DNA turn (10 bp). The 251 bp sequence was extended to 260 bp to correct for the twist underestimation of relaxed DNA by the AMBER parmBSC0 force field (31) (see the Supporting Material for the full sequence). DNA planar circles corresponding to four topoisomers ($\Delta Lk = -2, -1, 0, 1$) with/without the 16 bp triplex forming-oligomer (TFO) and with/without the DNA-binding domain of 434 repressor (Protein Data Bank (PDB): 2OR1 (30)) were then constructed using an in-house program (32). The 434-DNA crystallographic structure was bound to the minicircle by aligning the complex with its binding site.

MD simulations

The force field Amber ff99 (33) with parmBSC0 corrections for α and γ (34) and parm χOL4 correction for χ (35) was used to describe the DNA, and the force field ff99SB-ILDN (36,37) was used to describe the protein. Parameters for protonated cytosine present in the TFO were obtained from Soliva et al. (38). Using a multistage equilibration protocol described in Sutthibutpong et al. (39), the SANDER module within AMBER12 (29) was used to subject these starting structures to 13 ns of implicitly solvated MD using the generalized Born/solvent-accessible area method (40) at 300 K and 200 mM salt concentration, with the long-range electrostatic cutoff set to 100 Å. MD simulations with a continuum representation of the solvent rapidly explore conformational space in the absence of any frictional drag from collisions with water molecules (27) and can provide a comparable description of supercoiled DNA to explicitly solvated calculations in monovalent salt, so long as the DNA does not contain defects in the double helix (41). Therefore, restraints were applied to maintain the canonical H-bonding interactions for production runs in implicit solvent, as described in Irobalieva et al. (27). For the DNA bound to the 434 repressor, in four simulations we observed off-site interactions between positively charged amino acids and the negatively charged sugar-phosphate backbone, which were never present in explicit solvent. These conformations were discarded as they are potentially artifacts of the approximate solvent models (leaving 6 ns of implicitly solvated MD remaining). After discarding the first 3 ns for equilibration, the calculated average writhe for each topoisomer did not change by >0.1 turns for each topoisomer when the simulations were extended from 6 to 13 ns; consequently we considered the Writhe parameter (which represents the global shape of minicircles) to be adequately sampled by the implicitly solvated simulations (Fig. S1 in the Supporting Material) so that these provide suitably stable conformers for initiation of explicitly solvated calculations.

Following on from the implicit solvent runs, representative structures containing an equivalent configuration for each of the two binding sites to facilitate cross comparison in the presence and absence of ligands

were chosen for each topoisomer (see Fig. S2). For example, because the triplex binding site always lies at the apices for $\Delta Lk = -2$ in the absence of the third strand, we selected a configuration from the equivalent simulation containing the bound triplex as a starting structure, and removed the third strand before adding solvent (Fig. S2). All minicircles were solvated in 200 mM Na^+ and Cl^- counterions in TIP3P octahedral boxes (42). A quantity of 100 ns explicitly solvated MD simulations was performed using the GROMACS 4.5 program (43) with standard MD protocols (44) at 300 K.

Linear DNA fragments

A 56-mer fragment containing the triplex binding site and the repressor binding site was extracted from the 260 bp minicircle to analyze the properties of these bound/unbound sites on unconstrained linear DNA and to enable comparison with supercoiled minicircles. To reduce end effects, an additional 8 bp was added to both ends of each binding site (45) (see the Supporting Material). Four linear starting structures with/without the 16 bp TFO and with/without the DNA-binding domain of 434 repressor were explicitly solvated and subjected to 100-ns MD simulations using the protocols described previously in the Materials and Methods.

Trajectory analysis

Writhe calculations and other geometrical descriptions of the global molecular shape were performed by using the WrLINE molecular contour analysis tool (26). DNA Twist values were obtained with CURVES+ (46) and internal configurational energies were evaluated by the AMBER program MMPBSA (47). Ion densities around the DNA duplexes and radial distribution functions (RDF) were determined using the AMBER program PTRAJ (48). To assess the equilibration of the cation environment around the DNA, RDFs were calculated by increasing the length of time-windows from simulation trajectories (Fig. S3), showing good convergence after 60 ns. Consequently, much of the analysis (the ones not showing time series) was performed by considering only the last 40 ns of the trajectory. To locate potential crossing points, the smallest distance between two pieces of double-stranded DNA across the minicircle was calculated between each possible pair of nucleotides separated by at least 50 bp. Equivalently, the ability of the 434 repressor to stabilize a crossing point through a DNA-protein bridge was monitored by calculating the smallest distance between the protein-binding site and any nucleotide separated by at least 50 bp, and by the register angles between this site, the binding site, and the protein. A register angle close to zero indicates the protein faces toward the other DNA double strand or toward the center of the circle, while a register angle of ~180° indicates the protein faces away. The number of hydrogen bonds stabilizing the secondary recognition site of the observed DNA-434 bridges was determined using a distance cutoff of 3.5 Å between donor and acceptor atoms and an angle cutoff of 120°.

RESULTS

Implicit solvent MD shows global structural changes on ligand binding

The *Tw*/*Wr* partition, which dictates the global shape of the DNA, was firstly equilibrated with an implicit solvent model for each topoisomer with and without ligands (for 3 ns, followed by a 10 ns production run). MD simulations in implicit solvent allow rapid global structural rearrangements within the minicircles to be observed, even over limited MD timescales, because conformational fluctuations are accelerated by at least an order of magnitude when solvent damping is neglected (27). While the relaxed topoisomers remained predominantly circular, the supercoiled minicircles all adopted writhed configurations, with the $\Delta Lk = -2$, $\Delta Lk = -1$, and $\Delta Lk = +1$ having an average of ~1.5, 0.5, and 1 cross overs, respectively, for the naked DNA.

Fig. 1 shows representative configurations from the implicitly solvated MD simulations for the DNA alone and in the presence of ligands. Fig. 2 shows the radial positions of the triplex and protein binding sites in relation to the center of mass of the circle, which may be located either at the apices (far from the minicircle center of mass) or a site closer to the cross overs (near the center of mass). For the plectonemic $\Delta Lk = -2$ and $\Delta Lk = +1$ topoisomers, in the MD the poly-AG triplex binding site was seen to have a propensity to be located at the apices (see Fig. 1 *a*), which are significantly bent. While an analysis of the PDB (49,50) and long timescale MD simulations on short (12–16 bp) linear DNA fragments (51,52) have identified purine-purine steps as having intermediate flexibility, with TA steps being the most flexible, and GC the most rigid, this preference for the bent apices may be a specific property that emerges from the usually repetitive sequence associated with the triplex binding site. However, because the triplex is stiffer than naked DNA, the binding of the third strand shifts the preferred location of this sequence away from the bent apices, resulting in a global structural change within the minicircle (see Fig. 1 *b*). Because the third DNA strand carries additional negative charge, configurations where the triplex is located at a crossing point are unfavorable electrostatically; consequently, the triplex DNA has a propensity to be localized to the region between the cross overs and the apices of plectonemes. In the presence of the 434 repressor alone, the triplex binding site was located at the apex in the

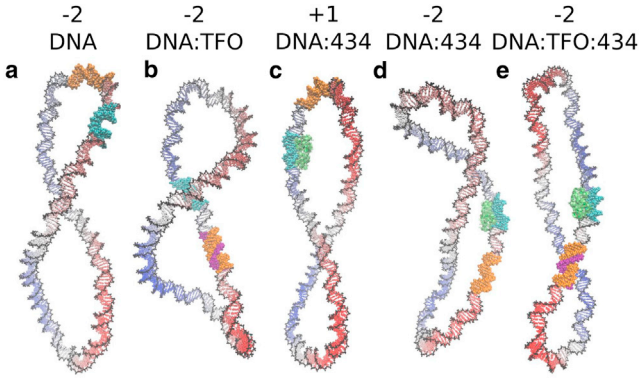

FIGURE 1 Representative structures from plectonemic ($\Delta Lk = -2, +1$ topoisomers) implicitly solvated simulations: (*a*) −2 for naked DNA, (*b*) −2 with TFO, (*c*) +1 with 434 repressor (434), (*d*) −2 with 434, and (*e*) −2 with both ligands. To enhance the 3D perspective, DNA regions colored in red are close to the reader, whereas those in blue are far away. The triplex-binding site is highlighted in yellow, the TFO in purple, the 434-binding site in cyan, and the 434 in green. To see this figure in color, go online.

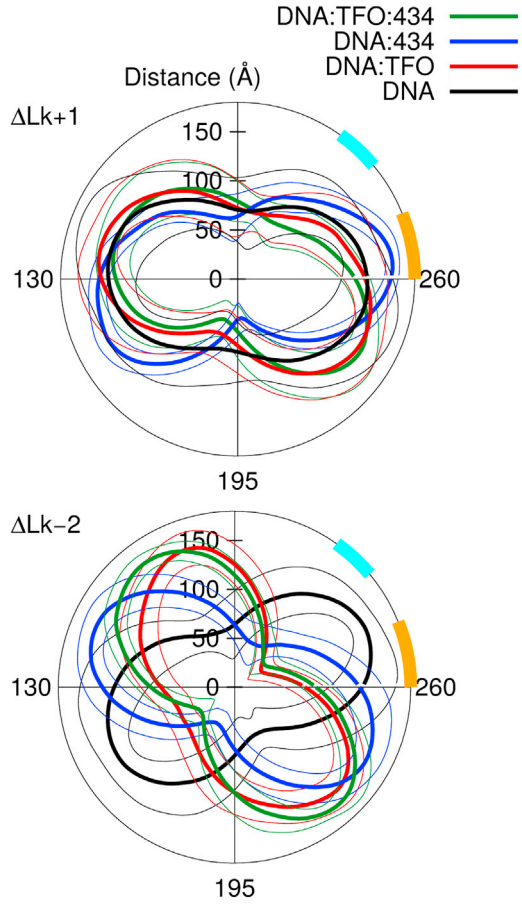

FIGURE 2 Distances between every residue (defined by the WrLINE molecular contour) and the center of mass obtained using the last 10 ns of the implicitly solvated simulations for the most supercoiled topoisomers ($\Delta Lk = -2, +1$) (values for $\Delta Lk = +1$ $DNA^{+}434$ and $\Delta Lk = -2$ DNA+TFO+434 topoisomers were calculated using the last 3 ns, as described in the Materials and Methods), with the corresponding margin of error calculated by average ± SD and represented by thin lines. Orange and cyan indicate the triplex and repressor binding sites, respectively. To see this figure in color, go online.

MD for the $\Delta Lk = +1$ topoisomer, as for the naked DNA (see Fig. 1 *c*). However, for the highly writhed $\Delta Lk = -2$ topoisomer, the bound 434 repressor was located at the crossover, where polar residues on the protein surface could provide electrostatic screening (Fig. 1 *d*). In the presence of both the triplex and the 434 repressor, in all cases the triplex was located away from the apices and the crossing points, which additionally placed the 434 repressor at a favorable position close to the crossing point (Fig. 1 *e*).

Close cross overs in plectonemes are stabilized by counterions

After equilibrating the *Tw*/*Wr* partition for each topoisomer using an implicit-solvent model, representative structures were solvated with explicit water and counterions (see Materials and Methods). The increase in solvent damping on addition of water retards global rearrangements of the minicircles sufficiently such that only local structural changes could be observed over the 100 ns timescales of these simulations. However, comparing the structures in Fig. S2 with Fig. 3 suggests that addition of explicit counterions leads to a compaction of the DNA in the MD simulations, implying that electrostatic screening is underestimated by the approximate implicit solvent model and that it is an important factor for DNA recognition as has been described in Cherstvy (53).

Fig. 4, *a* and *b*, shows the minimum distance between DNA cross overs and the measured *Wr* for the four topoisomers, respectively. The levels of superhelical stress simulated are clearly sufficient to pull together distal loop sites; while the minimum distance between any two distal sites is 100 Å in the relaxed topoisomer ($\Delta Lk = 0$), this is reduced to ~30 Å in the most negatively supercoiled topoisomer ($\Delta Lk = -2$). Because DNA basepairs are ~20 Å in width, a 30 Å separation between the helical axes of two previously distal sites can represent a distance of <10 Å between external backbone atoms. The value of $Wr = -1.5$ measured for the $\Delta Lk = -2$ indicates that most the minicircle conformers contain at least one crossing point for this topoisomer. These highly packed structures are stabilized by bridging interactions with the monovalent counterions that occur in an extended crossing point (indicated in *yellow* in Fig. 5). Similarly, compacted DNA minicircle structures have been observed by cryo-electron tomography experiments, which reported global conformations of highly compacted plectonemic minicircles resembling needles or rods, and other more complex structures (27). Moreover, a region of high counterion density can be observed at one apex of the doubly bound $\Delta Lk = -2$ topoisomer, where a kink defect further stabilizes the favorable arrangement of the triplex (away from apex and crossing point) and the 434 repressor (at the crossing). These simulations therefore show that the ability of DNA supercoiling to bring distal sites into close proximity is enhanced by the self-assembly of positive counterions at regions of high negative charge, which can also promote the formation of kink defects that may lock the global shape of the minicircle into a given conformer (27,44,54).

Plectonemes promote nonspecific protein-DNA interactions

Of the four simulations of plectonemic structures (e.g., the −2 and +1 topoisomers) with the bound 434 repressor protein, three showed additional nonspecific protein-DNA interactions with a site close to the diametrically opposite point on the circle from the protein binding site. This was never observed in the relaxed DNA. Examples of DNA-protein-DNA bridges observed in MD of the supercoiled topoisomers are shown in Fig. 6. These new interaction sites typically contain between 10 and 20 hydrogen bonds and

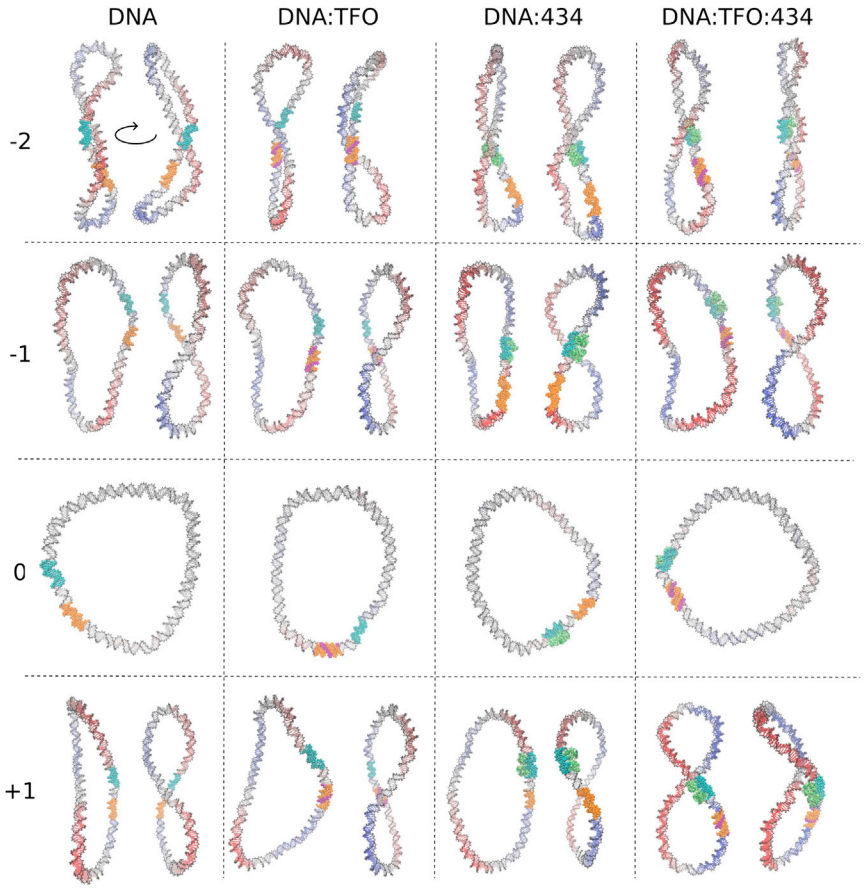

FIGURE 3 Two side views (at 90° clockwise rotation) of representative structures from the last 40 ns of explicitly solvated trajectories, constrained at different levels of superhelical stress ($\Delta Lk = -2$, -1, 0, $+1$ topoisomers) and with/without the presence of the TFO and the 434 repressor. Structures are color-coded as in Fig. 1. To see this figure in color, go online.

involve a broad range of amino acids and DNA backbone sites, indicating that these are highly unspecific in nature. Example hydrogen bonds donors included: polar amino acids (serine, asparagine, glutamine, tryptophan, and glycine), positively charged residues (arginine and glycine) and even an example of a hydrogen bond with the backbone of an apolar glycine was observed. In the doubly bound $\Delta Lk = -2$ minicircle, in which the triplex resides in its preferred site between the apex and the crossing point, and a kink defect formed at one apex, we observe that nonspecific protein-DNA interaction occurs after only 20 ns compared to 60 ns in the presence of the repressor (see Fig. 7). Moreover, there was an increase in the number of nonspecific hydrogen bond contacts between the 434 repressor and the distal site from ~15 to 20 (Fig. 7). We hypothesize that kink formation, triplex binding, and nonspecific interactions between the 434 repressor and the DNA occur cooperatively in this plectoneme.

For the $\Delta Lk = +1$ topoisomer, DNA-protein-DNA bridges were only observed in the simulation containing both the triplex and the 434 repressor. Protein-DNA bridges were also not observed in simulations of the $\Delta Lk = -1$ topoisomers. In these simulations, the protein-minicircle complex adopted conformations where the protein was on the outside of the minicircle so that secondary binding interactions were sterically inaccessible, illustrating that the registry of the circle (e.g., the degree of freedom associated with rotating the helix around its central axis) can also be important in modulating DNA-binding interactions in complex topologies (Fig. 7). While changes in register angle are indeed sampled more extensively during the implicitly solvated MD (see Fig. S4), the additional compaction of plectonemes in the presence of explicit counterions is required to bring the DNA sufficiently close for these bridging interactions to be encountered. This coupling between the details of the counterion environment and the global shape of the DNA makes conformational sampling particularly computationally challenging, and indeed kinetic trapping of DNA conformations on a surface by the choice of solvent environment has been demonstrated by AFM experiments (55). Although this implies that caution is necessary for interpreting MD simulations of writhed DNA minicircles, due to the differences in timescale and environment conditions that may be accessible in simulations and future experiments, our trajectories show repeatedly the potential of the 434 repressor DNA-binding domain to form a protein-bridge across a supercoiled DNA loop through nonspecific contacts. We propose that this interaction, which is driven by favorable electrostatics and by the plectonemic

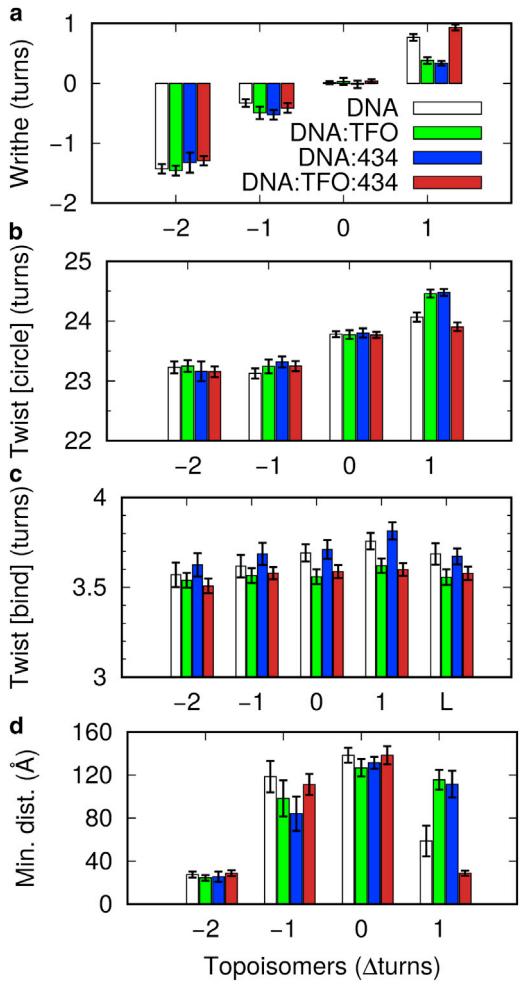

FIGURE 4 Writhe (*a*), total twist for the whole minicircle (*b*) and for the fragment comprised by both binding sites, and the central DNA turn (*c*) evaluated in DNA helical turns. (*d*) Minimum distance across the minicircle measured by the WrLINE helical axis between the two closest basepairs linearly separated at least by 50 bp. Averages and corresponding SDs (*error bars*) were obtained over the last 40 ns of trajectories using the explicit solvent model. To see this figure in color, go online.

closeness of two double helices, is an example of biological communication in 3D space.

Local structural changes on ligand binding

Molecular helical *Tw* averages for the 40 bp fragment composed of the two binding sites and the central helical turn show a strong variation in the presence/absence of the ligands (Fig. 4 *c*). While the binding of the 434 repressor promotes a variable degree of overtwisting (13) depending on the superhelical density, the TFO imposes low *Tw* of ~31°/bp step (56). However, alterations of local DNA structure caused by binding of either the TFO or the repressor alone are insufficient to induce significant conformational changes in the nearby binding site relative to SD, as indicated by the configurational energies presented in Fig. S5.

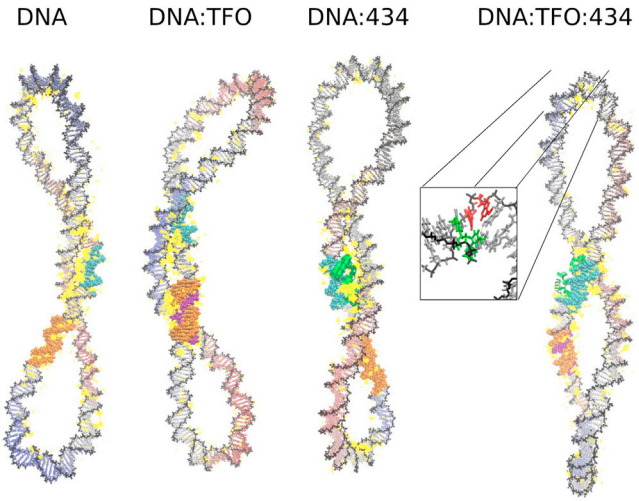

FIGURE 5 Averaged structures of the last 10 ns of explicitly solvated MD simulations of the $\Delta Lk = -2$ topoisomers together with Na^+-density maps from the same trajectory fragment showing an occupancy of ~3 times or greater the bulk concentration (in *yellow*). Structures are color-coded as Fig. 1. To see this figure in color, go online.

Moreover, local changes in helical twist at the binding sites are compensated by fluctuations in other individual steps along the minicircle and, therefore, they do not detectably alter the global *Tw*/*Wr* partition (Fig. 4 *b*). The simulations of the $\Delta Lk = +1$ topoisomer (see Fig. 4 *b*), however, suggest that the presence of a well-oriented protein could provide a mechanism for modifying this partition by efficiently screening the electrostatic repulsion between the negatively charged backbones of DNA. Therefore, in these simulations of minicircle DNA, we find that 3D long-range communication due to the complex topology of closed circular DNA makes a more significant contribution than 1D communication between distal binding sites.

CONCLUSIONS

Our MD simulations have shown that the binding of two distant ligands to supercoiled DNA is determined by a subtle interplay of DNA mechanics and electrostatics at the local level, which is capable of introducing global topological changes within the whole minicircle, thus, establishing a mechanism to transfer conformational information beyond the simple 1D order of regulatory elements placed sequentially on the DNA double helix. A balance of favorable and unfavorable electrostatic interactions, together with an alteration of the DNA elastic profile, determined which interactions occurred at the atomistic level, and the overall global position of the two ligands in the supercoiled minicircles. The binding of the triplex DNA introduces additional negative charge and stiffness, preventing it from occupying the crossing points and apices of plectonemes. Attractive electrostatic interactions between the DNA and positively charged sodium counterions allow sufficiently

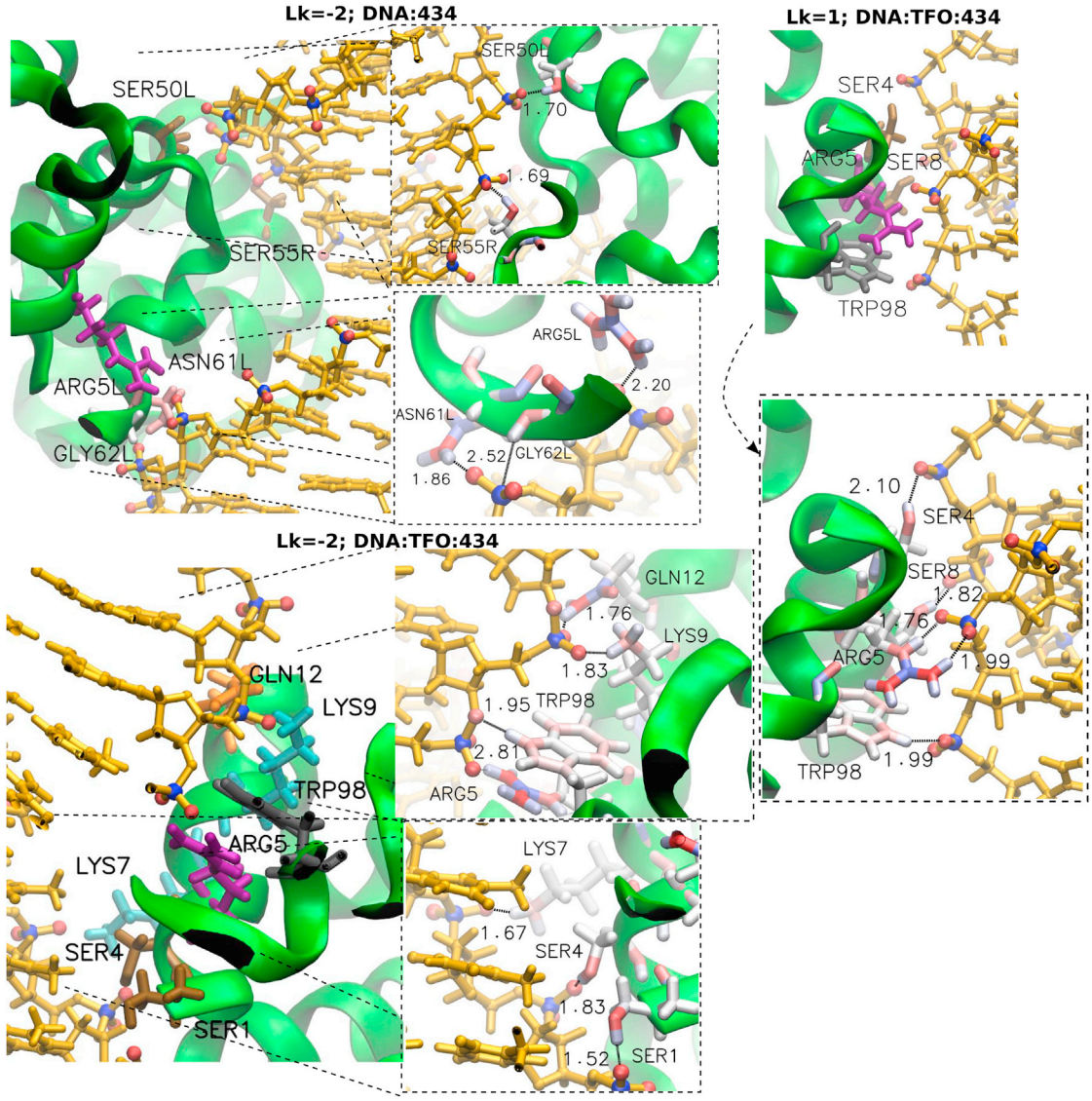

FIGURE 6 Detailed views of DNA: 434-repressor secondary recognition sites obtained from representative structures of the $\Delta Lk = -2$ topoisomer with the TFO and the 434 repressor (extracted approximately at 100 ns), the $\Delta Lk = -2$ topoisomer with the 434 repressor (at 90 ns), and the $\Delta Lk = +1$ topoisomer with the TFO and the 434 repressor (at 20 ns). The DNA (*yellow*), the core protein (*green*), and interacting amino acids (*brown*, serine; *purple*, arginine; *cyan*, lysine; *pink*, asparagine; *orange*, glutamine; *black*, tryptophan, and *white*, glycine). Closeups show atom charge (*blue* is positive and *red* is negative) and hydrogen bond distances. To see this figure in color, go online.

close contacts between distal sites within plectonemes that additional nonspecific interactions can form between the DNA and a bound protein, so long as the register angle for rotation along the axis of the helix places the protein on the inside of the minicircle. For the most compact $\Delta Lk = -2$ topoisomer, we observed a kink defect at the apices of the plectoneme in the presence of explicit counterions, the triplex and the protein.

In these minicircles, our choice of relative positions of the two binding sites enables the 434 repressor protein and the triplex to simultaneously adopt preferred locations. We hypothesize that minicircle sequences, where the binding site separations are chosen to disrupt this positive cooperativity, would have a lower affinity for the two ligands. Additional stabilization of these favorable configurations by kink formation was also observed in highly supercoiled DNA. If the probability of kinking at the apices is increased by the additional DNA compaction induced by cooperative binding by the triplex and the 434 repressor, then, we would expect that minicircle sequences in which triplex and repressor binding is negatively cooperative would also have a reduced propensity to form kink defects at the apices. Our calculations show that even if the binding of multiple ligands to distant sites occurs independently in linear sequences, closed topologies may promote cooperativity that has a rich dependence on the degree of DNA supercoiling.

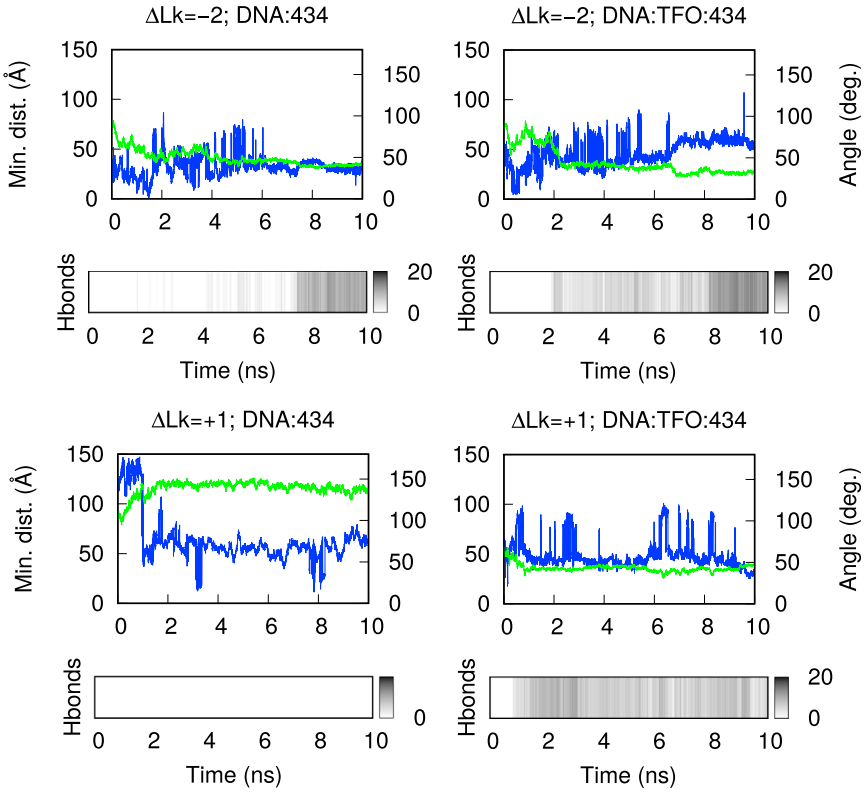

FIGURE 7 Time evolution of the crossing distance between the 434 repressor binding site and the closest basepair linearly separated by at least 50 bp (*green*), together with the corresponding register angle (defined by this site, the binding site, and the protein, *blue*) from the explicitly solvated simulations of supercoiled minicircles with only the protein bound (*left*) or both ligands (*right*). The number of hydrogen bonds presented in the secondary recognition (*gray-scaled heat maps*) is counted according to a distance cutoff of 3.5 Å between donor and acceptor atoms and an angle cutoff of 120°. To see this figure in color, go online.

SUPPORTING MATERIAL

Supporting Materials and Methods and five figures are available at http://www.biophysj.org/biophysj/supplemental/S0006-3495(16)34340-5.

AUTHOR CONTRIBUTIONS

A.N. designed and performed the research, and wrote the article; and A.M. and S.A.H. designed the research and wrote the article.

ACKNOWLEDGMENTS

We thank Andrew D. Bates, Bart W. Hoogenboom, Alice Pyne, and Michael M. Piperakis for useful discussions and comments. This work made use of time on the ARC2 supercomputer facility at the University of Leeds.

A.N. is supported by the Engineering and Physical Sciences Research Council, UK ((EPSRC) grant No. EP/N027639/1); S.A.H. and A.M. acknowledge support from the Biotechnology and Biological Sciences Research Council, UK ((BBSRC) grant No. BB/I019472/1). A.M. is also supported by the BBSRC (grant No. BB/J004561/1) and the John Innes Foundation. Time on ARCHER was granted via the UK High-End Computing Consortium for Biomolecular Simulation, HECBioSim (http://www.hecbiosim.ac.uk), supported by the EPSRC (grant No. EP/L000253/1).

REFERENCES

1. Dorman, C. J. 2011. Regulation of transcription by DNA supercoiling in *Mycoplasma genitalium*: global control in the smallest known self-replicating genome. *Mol. Microbiol.* 81:302–304.
2. Liu, L. F., and J. C. Wang. 1987. Supercoiling of the DNA template during transcription. *Proc. Natl. Acad. Sci. USA.* 84:7024–7027.
3. Teves, S. S., and S. Henikoff. 2014. Transcription-generated torsional stress destabilizes nucleosomes. *Nat. Struct. Mol. Biol.* 21:88–94.
4. Papillon, J., J.-F. Ménétret, …, V. Lamour. 2013. Structural insight into negative DNA supercoiling by DNA gyrase, a bacterial type 2A DNA topoisomerase. *Nucleic Acids Res.* 41:7815–7827.
5. Bates, A. D., and A. Maxwell. 1989. DNA gyrase can supercoil DNA circles as small as 174 base pairs. *EMBO J.* 8:1861–1866.
6. Bancaud, A., N. Conde e Silva, …, J.-L. Viovy. 2006. Structural plasticity of single chromatin fibers revealed by torsional manipulation. *Nat. Struct. Mol. Biol.* 13:444–450.
7. Zechiedrich, E. L., A. B. Khodursky, …, N. R. Cozzarelli. 2000. Roles of topoisomerases in maintaining steady-state DNA supercoiling in *Escherichia coli*. *J. Biol. Chem.* 275:8103–8113.
8. Norouzi, D., and V. B. Zhurkin. 2015. Topological polymorphism of the two-start chromatin fiber. *Biophys. J.* 108:2591–2600.
9. Bates, A. D., and A. Maxwell. 2005. DNA Topology. Oxford University Press, Oxford, London, UK.
10. Sutthibutpong, T., C. Matek, …, S. A. Harris. 2016. Long-range correlations in the mechanics of small DNA circles under topological stress revealed by multi-scale simulation. *Nucleic Acids Res.* 44:9121–9130.
11. Mitchell, J. S., and S. A. Harris. 2013. Thermodynamics of writhe in DNA minicircles from molecular dynamics simulations. *Phys. Rev. Lett.* 110:148105.
12. Rohs, R., S. M. West, …, B. Honig. 2009. The role of DNA shape in protein-DNA recognition. *Nature.* 461:1248–1253.
13. Koudelka, G. B. 1998. Recognition of DNA structure by 434 repressor. *Nucleic Acids Res.* 26:669–675.
14. Maxwell, A., N. P. Burton, and N. O'Hagan. 2006. High-throughput assays for DNA gyrase and other topoisomerases. *Nucleic Acids Res.* 34:e104.

15. Kouzine, F., J. Liu, …, D. Levens. 2004. The dynamic response of upstream DNA to transcription-generated torsional stress. *Nat. Struct. Mol. Biol.* 11:1092–1100.
16. Lilley, D. M. J., and C. F. Higgins. 1991. Local DNA topology and gene expression: the case of the leu-500 promoter. *Mol. Microbiol.* 5:779–783.
17. Sobetzko, P. 2016. Transcription-coupled DNA supercoiling dictates the chromosomal arrangement of bacterial genes. *Nucleic Acids Res.* 44:1514–1524.
18. Kim, S., E. Broströmer, …, X. S. Xie. 2013. Probing allostery through DNA. *Science.* 339:816–819.
19. Liu, Y., V. Bondarenko, …, V. M. Studitsky. 2001. DNA supercoiling allows enhancer action over a large distance. *Proc. Natl. Acad. Sci. USA.* 98:14883–14888.
20. Normanno, D., F. Vanzi, and F. S. Pavone. 2008. Single-molecule manipulation reveals supercoiling-dependent modulation of lac repressor-mediated DNA looping. *Nucleic Acids Res.* 36:2505–2513.
21. Norregaard, K., M. Andersson, …, L. B. Oddershede. 2013. DNA supercoiling enhances cooperativity and efficiency of an epigenetic switch. *Proc. Natl. Acad. Sci. USA.* 110:17386–17391.
22. Norregaard, K., M. Andersson, …, L. B. Oddershede. 2014. Effect of supercoiling on the λ switch. *Bacteriophage.* 4:e27517.
23. Leng, F., B. Chen, and D. D. Dunlap. 2011. Dividing a supercoiled DNA molecule into two independent topological domains. *Proc. Natl. Acad. Sci. USA.* 108:19973–19978.
24. D'Annessa, I., A. Coletta, …, A. Desideri. 2014. Simulations of DNA topoisomerase 1B bound to supercoiled DNA reveal changes in the flexibility pattern of the enzyme and a secondary protein-DNA binding site. *Nucleic Acids Res.* 42:9304–9312.
25. Noy, A., T. Sutthibutpong, and S. A. Harris. 2016. Protein/DNA interactions in complex DNA topologies: expect the unexpected. *Biophys. Rev.* 8:233–243.
26. Sutthibutpong, T., S. A. Harris, and A. Noy. 2015. Comparison of molecular contours for measuring writhe in atomistic supercoiled DNA. *J. Chem. Theory Comput.* 11:2768–2775.
27. Irobalieva, R. N., J. M. Fogg, …, L. Zechiedrich. 2015. Structural diversity of supercoiled DNA. *Nat. Commun.* 6:8440.
28. Fogg, J. M., N. Kolmakova, …, E. L. Zechiedrich. 2006. Exploring writhe in supercoiled minicircle DNA. *J. Phys. Condens. Matter.* 18:S145–S159.
29. Case, D., T. Darden, …, P. Kollman. 2012. AMBER 12. ambermd.org.
30. Aggarwal, A. K., D. W. Rodgers, …, S. C. Harrison. 1988. Recognition of a DNA operator by the repressor of phage 434: a view at high resolution. *Science.* 242:899–907.
31. Bates, A. D., A. Noy, …, A. Maxwell. 2013. Small DNA circles as probes of DNA topology. *Biochem. Soc. Trans.* 41:565–570.
32. Sutthibutpong, T., A. Noy, and S. Harris. 2016. Atomistic molecular dynamics simulations of DNA minicircle topoisomers: a practical guide to setup, performance, and analysis. *In* Chromosome Architecture: Methods and Protocols. C. M. Leake, editor. Springer, New York, NY, pp. 195–219.
33. Cheatham, T. E., 3rd, P. Cieplak, and P. A. Kollman. 1999. A modified version of the Cornell et al. force field with improved sugar pucker phases and helical repeat. *J. Biomol. Struct. Dyn.* 16:845–862.
34. Pérez, A., I. Marchán, …, M. Orozco. 2007. Refinement of the AMBER force field for nucleic acids: improving the description of α/γ conformers. *Biophys. J.* 92:3817–3829.
35. Krepl, M., M. Zgarbová, …, J. Sponer. 2012. Reference simulations of noncanonical nucleic acids with different χ variants of the AMBER force field: quadruplex DNA, quadruplex RNA and Z-DNA. *J. Chem. Theory Comput.* 8:2506–2520.
36. Hornak, V., R. Abel, …, C. Simmerling. 2006. Comparison of multiple Amber force fields and development of improved protein backbone parameters. *Proteins.* 65:712–725.
37. Lindorff-Larsen, K., S. Piana, …, D. E. Shaw. 2010. Improved side-chain torsion potentials for the Amber ff99SB protein force field. *Proteins.* 78:1950–1958.
38. Soliva, R., F. J. Luque, and M. Orozco. 1999. Can G-C Hoogsteen-wobble pairs contribute to the stability of d(G. C-C) triplexes? *Nucleic Acids Res.* 27:2248–2255.
39. Sutthibutpong, T., A. Noy, and S. A. Harris. 2015. Atomistic molecular dynamics simulations of DNA minicircle topoisomers: a practical guide to setup, performance and analysis. *Methods Mol. Biol.* 1431:195–219.
40. Tsui, V., and D. A. Case. 2000–2001. Theory and applications of the generalized Born solvation model in macromolecular simulations. *Biopolymers.* 56:275–291.
41. Mitchell, J., and S. Harris. 2011. Testing the use of implicit solvent in the molecular dynamics modelling of DNA flexibility. *Prog. Theor. Phys. Suppl.* 191:96–108.
42. Smith, D. E., and L. X. Dang. 1994. Computer simulations of NaCl association in polarizable water. *J. Chem. Phys.* 100:3757–3766.
43. Hess, B., C. Kutzner, …, E. Lindahl. 2008. GROMACS 4: algorithms for highly efficient, load-balanced, and scalable molecular simulation. *J. Chem. Theory Comput.* 4:435–447.
44. Mitchell, J. S., C. A. Laughton, and S. A. Harris. 2011. Atomistic simulations reveal bubbles, kinks and wrinkles in supercoiled DNA. *Nucleic Acids Res.* 39:3928–3938.
45. Noy, A., and R. Golestanian. 2012. Length scale dependence of DNA mechanical properties. *Phys. Rev. Lett.* 109:228101.
46. Lavery, R., M. Moakher, …, K. Zakrzewska. 2009. Conformational analysis of nucleic acids revisited: Curves+. *Nucleic Acids Res.* 37:5917–5929.
47. Miller, B. R., 3rd, T. D. McGee, Jr., …, A. E. Roitberg. 2012. MMPBSA.py: an efficient program for end-state free energy calculations. *J. Chem. Theory Comput.* 8:3314–3321.
48. Roe, D. R., and T. E. Cheatham, 3rd. 2013. PTRAJ and CPPTRAJ: software for processing and analysis of molecular dynamics trajectory data. *J. Chem. Theory Comput.* 9:3084–3095.
49. Olson, W. K., A. A. Gorin, …, V. B. Zhurkin. 1998. DNA sequence-dependent deformability deduced from protein-DNA crystal complexes. *Proc. Natl. Acad. Sci. USA.* 95:11163–11168.
50. Zheng, G., A. V. Colasanti, …, W. K. Olson. 2010. 3DNALandscapes: a database for exploring the conformational features of DNA. *Nucleic Acids Res.* 38:D267–D274.
51. Ivani, I., P. D. Dans, …, M. Orozco. 2016. Parmbsc1: a refined force field for DNA simulations. *Nat. Methods.* 13:55–58.
52. Pasi, M., J. H. Maddocks, …, R. Lavery. 2014. μABC: a systematic microsecond molecular dynamics study of tetranucleotide sequence effects in B-DNA. *Nucleic Acids Res.* 42:12272–12283.
53. Cherstvy, A. G. 2011. Electrostatic interactions in biological DNA-related systems. *Phys. Chem. Chem. Phys.* 13:9942–9968.
54. Matek, C., T. E. Ouldridge, …, A. A. Louis. 2015. Plectoneme tip bubbles: coupled denaturation and writhing in supercoiled DNA. *Sci. Rep.* 5:7655.
55. Billingsley, D. J., J. Kirkham, …, N. H. Thomson. 2010. Atomic force microscopy of DNA at high humidity: irreversible conformational switching of supercoiled molecules. *Phys. Chem. Chem. Phys.* 12:14727–14734.
56. Radhakrishnan, I., and D. J. Patel. 1994. DNA triplexes: solution structures, hydration sites, energetics, interactions, and function. *Biochemistry.* 33:11405–11416.